

High-Pressure Chemistry

How to cite: *Angew. Chem. Int. Ed.* **2020**, 59, 17533–17539

International Edition: doi.org/10.1002/anie.202001635

German Edition: doi.org/10.1002/ange.202001635

Pressure-Suppressed Carrier Trapping Leads to Enhanced Emission in Two-Dimensional Perovskite (HA)₂(GA)Pb₂I₇ **HPSTAR**
962-2020

Songhao Guo, Yongsheng Zhao, Kejun Bu, Yongping Fu, Hui Luo, Mengting Chen, Matthew P. Hautzinger, Yingqi Wang, Song Jin, Wenge Yang,* and Xujie Lü*

Abstract: A remarkable PL enhancement by 12 fold is achieved using pressure to modulate the structure of a recently developed 2D perovskite (HA)₂(GA)Pb₂I₇ (HA = *n*-hexylammonium, GA = guanidinium). This structure features a previously unattainable, extremely large cage. In situ structural, spectroscopic, and theoretical analyses reveal that lattice compression under a mild pressure within 1.6 GPa considerably suppresses the carrier trapping, leading to significantly enhanced emission. Further pressurization induces a non-luminescent amorphous yellow phase, which is retained and exhibits a continuously increasing band gap during decompression. When the pressure is released to 1.5 GPa, emission can be triggered by above-band gap laser irradiation, accompanied by a color change from yellow to orange. The obtained orange phase could be retained at ambient conditions and exhibits two-fold higher PL emission compared with the pristine (HA)₂(GA)Pb₂I₇.

Introduction

Organic–inorganic halide perovskites possessing unique lattice and electronic structures have been intensively investigated for applications such as solar cells, light-emitting diodes (LEDs), lasers, and photodetectors.^[1] A major obstacle in the development of three-dimensional (3D) ABX₃ perovskites is the very limited accessibility of their compositions as only three A-site cations of Cs⁺, CH₃NH₃⁺ (MA), and HC(NH₂)₂⁺ (FA) are able to maintain the stable 3D corner-sharing perovskite framework.^[2] Reduction of the structural dimensionality not only grants access to numerous material systems but also allows for the fine-tuning of their optoelectronic properties.^[2b,3] The most prominent examples are layered 2D Ruddlesden–Popper (RP) halide perovskites, which adopt a different compositional and structural formula of LA₂A_{*n*-1}B_{*n*}X_{3*n*+1},^[3a,4] where LA is the interlayer organic cation and *n* is the number of inorganic BX₆ octahedral layers.

Owing to the strong quantum and dielectric confinements, excitons can be stabilized at room temperature with large binding energies of hundreds of meV in 2D RP perovskites,^[3a,4b] making them more promising for light-emitting applications.^[5] However, their emission efficiency is still far from satisfactory, and the underlying mechanisms have not been well established yet. The rational design of new and more efficient 2D perovskites calls for better fundamental understanding such as how structural deformation affects the optical properties.

In 2D perovskite structures, many choices can be made for LA cations and the selection of A-site cations is also expanded.^[3a,6] Guanidinium [C(NH₂)₃]⁺ (GA⁺) has been reported as a larger A cation that can be fitted into the RP perovskite cage,^[6] which relaxes the Goldschmidt tolerance factor and increases the compositional tunability. The incorporation of such over-sized GA⁺ expands the perovskite cage and induces a large octahedral distortion in the inorganic framework, which would lead to a strong exciton–phonon interaction that creates a high degree of charge carrier trapping in the 2D perovskites.^[6,7] Importantly, the significantly expanded cage of the GA perovskite, setting it apart from other 2D perovskites, would enable us to reach the unexplored structural region which offers more tuning opportunities for fundamental study upon applying external stimuli such as temperature and pressure.

Pressure, as an effective tuning knob, can not only effectively adjust the structures and properties of materials without changing their chemical compositions but also enable the exploration of novel materials with emergent and/or enhanced properties.^[8] The organic–inorganic hybrid nature and soft lattices of halide perovskites make the pressure effects much more profound, especially for the variation of carrier trapping that is critical for optoelectronic properties. Recently, pressure-induced emission in halide perovskites was proposed by Zou et al.,^[9] which is due to the notable changes in structures under pressure. Studies on pressure-induced behaviors of 2D perovskites have recently begun and photoluminescence (PL) performance can be effectively adjusted by pressure,^[10] but the relationship between carrier trapping and PL intensity has not been well understood. Furthermore, the property evolution during decompression has rarely been examined, which is very important for ambient-pressure applications. In this work, we employ pressure to modulate the highly distorted 2D GA-based perovskite (HA)₂(GA)Pb₂I₇. The variations of optical and structural properties under high pressure were systematically investigated using in situ PL, UV/Vis absorption, Raman

[*] S. Guo, Y. Zhao, K. Bu, H. Luo, M. Chen, Y. Wang, Prof. W. Yang, Prof. X. Lü
Center for High Pressure Science and Technology Advanced Research (HPSTAR), Shanghai 201203 (P. R. China)
E-mail: yangwg@hpstar.ac.cn
xujie.lu@hpstar.ac.cn

Y. Fu, M. P. Hautzinger, Prof. S. Jin
Department of Chemistry, University of Wisconsin–Madison
Madison, WI 53706 (USA)

Supporting information and the ORCID identification number(s) for the author(s) of this article can be found under:
<https://doi.org/10.1002/anie.202001635>.

spectroscopy, and synchrotron X-ray diffraction (XRD), as well as first-principles calculations. Notably, we found significantly enhanced emission and reduced carrier trapping in $(\text{HA})_2(\text{GA})\text{Pb}_2\text{I}_7$ under pressure. We also pay attention to the property changes during decompression as well as the difference of the sample before and after high-pressure treatments. Strikingly, an irreversible process was observed and a new phase of $(\text{HA})_2(\text{GA})\text{Pb}_2\text{I}_7$ with reduced carrier trapping was obtained from the recrystallization of the pressure-induced amorphous phase, exhibiting a significantly enhanced emission.

Results and Discussion

Pressure-dependent emission property of $(\text{HA})_2(\text{GA})\text{Pb}_2\text{I}_7$ was measured using in situ PL spectroscopy during compression and decompression. At ambient conditions, $(\text{HA})_2(\text{GA})\text{Pb}_2\text{I}_7$ shows a relatively weak emission centered at around 570 nm with an asymmetric line-shape, where the lower energy side emission is mainly attributed to the radiative recombination of trapped carriers.^[7] The confined

excitons within the multiple quantum wells of the 2D perovskite will suppress the dissociation of electron-hole pairs to free carriers, therefore high emission efficiency via geminate recombination in 2D perovskite was expected.^[3b,7] However, the PL intensity of $(\text{HA})_2(\text{GA})\text{Pb}_2\text{I}_7$ is about one order of magnitude lower than that of the MA counterpart $(\text{HA})_2(\text{MA})\text{Pb}_2\text{I}_7$,^[6] suggesting a more pronounced nonradiative recombination through the phonon-assisted channel in the GA compound. This is probably due to its lower crystallographic symmetry ($P\bar{1}$ and $C2/c$ for GA and MA compounds, respectively) and larger distortions of the Pb-I inorganic sublattice, indicating the stronger exciton-phonon coupling in $(\text{HA})_2(\text{GA})\text{Pb}_2\text{I}_7$.^[6] Interestingly, the PL intensity of $(\text{HA})_2(\text{GA})\text{Pb}_2\text{I}_7$ exhibits a sharp increase during compression and reaches a 12-fold enhancement at 1.59 GPa compared with that at ambient conditions (Figure 1a; Supporting Information, Figure S1). Then, the PL intensity exhibits a gradual decrease beyond 1.6 GPa and eventually disappears at 9.48 GPa, which is mainly due to the appearance of structural disorder.^[8d,9b,11] Furthermore, the fluorescence micrographs at different pressures in the chamber of a diamond anvil cell (DAC) clearly demonstrate the changes in

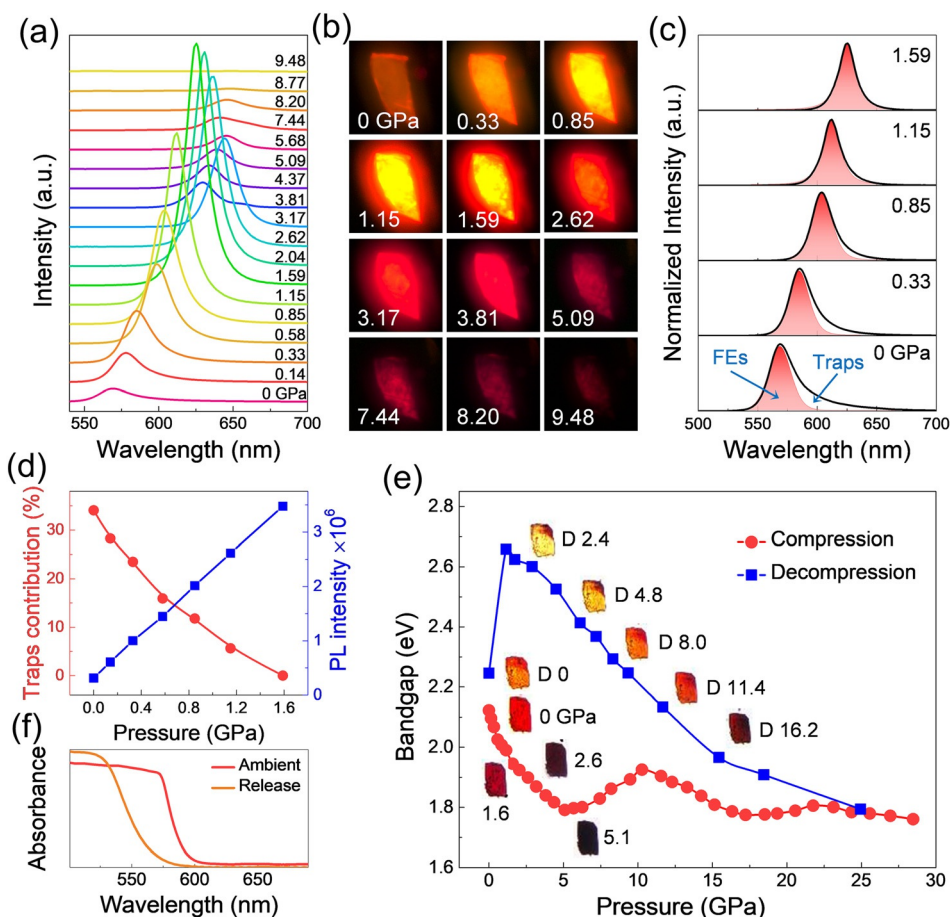


Figure 1. In situ optical properties of $(\text{HA})_2(\text{GA})\text{Pb}_2\text{I}_7$ single crystals under high pressures. a) PL spectra excited by 405 nm laser during compression. b) Fluorescence micrographs at selected pressures. c) The fitting curves of the PL spectra under selected pressures, where the red and white regions are the emission of the free excitons (FEs) and trapped states (Traps), respectively. d) Contribution of trapped states emission and the PL intensity as a function of pressure. e) Bandgap evolution as a function of pressure and the corresponding optical images. f) Absorption spectra before and after pressure treatment up to 30 GPa.

emission brightness (Figure 1 b; Supporting Information, Figure S2).

The PL spectra were fitted to estimate the contributions of emission from free excitons (FEs, photo-excited electron–hole pairs) and trapped states at each pressure. As shown in Figure 1 c and the Supporting Information, Figure S3, there is a significant contribution from the trapped states in the PL spectrum of $(\text{HA})_2(\text{GA})\text{Pb}_2\text{I}_7$ at ambient pressure, which likely leads to its weaker PL intensity. Strikingly, the contribution of emission from the trapped states gradually decreases upon compression. Subsequently, the trap-state emission totally disappeared at 1.59 GPa, where the brightest PL was achieved. Figure 1 d presents the contribution from trap-state emission and the total PL intensity as a function of pressure, which confirms the strong correlation between the suppression of carrier trapping and the increase of PL intensity. It has been reported that the decrease of the energetic barrier between the free excitons and the trapped states would result in the reduction of carrier trapping.^[7,12] The change in the energetic barrier of $(\text{HA})_2(\text{GA})\text{Pb}_2\text{I}_7$ is likely caused by modulation and regulation of the Pb–I inorganic sublattice by pressure towards a reduced distortion, which would dramatically affect the exciton-phonon interaction.^[6,10c]

To explore the band structure evolution, in situ UV/Vis absorption spectroscopy was utilized to measure the band gap of $(\text{HA})_2(\text{GA})\text{Pb}_2\text{I}_7$ under high pressure (Supporting Information, Figure S4). At ambient conditions, a steep absorption edge is observed at 580 nm which is consistent with the previous report.^[6] As summarized in Figure 1 e, the band gap decreases initially up to 5.1 GPa with the color of the crystal changing from red to black, followed by an increase from 5.1 GPa to 10.3 GPa, and then gradually decreases with further pressurization. These trends of band gap narrowing followed by widening upon compression have been reported in other 2D lead halide perovskites, and are probably due to pressure-induced atomic distortion and amorphization.^[10a,d] It is worth noting that the band gap of $(\text{HA})_2(\text{GA})\text{Pb}_2\text{I}_7$ can

recover to its original value following the compression path when the pressure is released from a relatively low pressure, such as 13 GPa (Supporting Information, Figures S5 and S6). However, when the pressure is released from a higher pressure of 30 GPa, it goes through a dramatically different and anomalous process during decompression. The band gap values of $(\text{HA})_2(\text{GA})\text{Pb}_2\text{I}_7$ during decompression are considerably larger than those during compression, shown as yellow in the optical images (inset in Figure 1 e and the Supporting Information, Figure S7). The band gap at about 1 GPa during decompression is 2.66 eV which is 33% larger than that during compression (2.0 eV). After totally releasing the pressure, the sample changes from yellow to orange with a band gap of 2.25 eV, which is 6% larger than the band gap of the original sample in red (Figure 1 f). The observation of the irreversible decompression process suggests dramatic changes in the lattice and electronic structure when a critical pressure is reached.^[8b,10b,13] Materials with irreversible pressure-induced transitions are desired if we want to maintain the emergent and/or enhanced high-pressure properties when the pressure is released, which is of great significance for further characterization and materials design.

To investigate the structural variations behind the anomalous behaviors of the optical properties, in situ synchrotron XRD measurement was performed on $(\text{HA})_2(\text{GA})\text{Pb}_2\text{I}_7$ up to 30 GPa, as shown in Figure 2 a and the Supporting Information, Figure S8. At ambient conditions, $(\text{HA})_2(\text{GA})\text{Pb}_2\text{I}_7$ crystallizes in a triclinic space group $P\bar{1}$ with $a = 8.8195(14)$ Å, $b = 9.0300(15)$ Å, $c = 21.699(4)$ Å, $\alpha = 79.965(13)^\circ$, $\beta = 87.341(9)^\circ$, and $\gamma = 89.986(10)^\circ$. As shown in Figure 2 b, it possesses a molecularly 2D layered structure that features inorganic anionic layers made of two-layer octahedra $[\text{Pb}_2\text{I}_7]^{3-}$, which are separated by the $[\text{HA}]^+$ organic cationic layers. The $[\text{Pb}_2\text{I}_7]^{3-}$ inorganic layers are constructed by corner-sharing $[\text{PbI}_6]^{4-}$ octahedra, where the GA cations occupy the A site cavity of the perovskite cage. The large GA cations lead to an enormous expansion and large distortion of

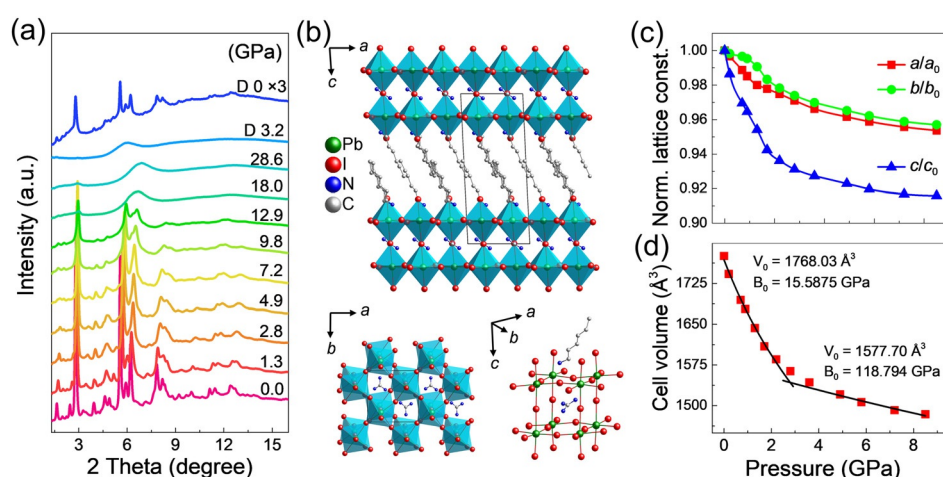


Figure 2. In situ structural characterizations of $(\text{HA})_2(\text{GA})\text{Pb}_2\text{I}_7$ under high pressures. a) Synchrotron X-ray diffraction patterns at selected pressures. b) Crystal structure at ambient conditions along different crystallographic axes. c) Compressibility along different lattice axes. d) Unit-cell volume as a function of pressure. Second-order Birch-Murnaghan equation of states (EOS) fitting curves are shown as black lines.

the inorganic framework, giving rise to the lower crystallographic symmetry.

During compression, all diffraction peaks shift to higher angles due to the lattice contraction. The crystal structures of $(\text{HA})_2(\text{GA})\text{Pb}_2\text{I}_7$ are refined by the Rietveld method at selected pressures of 0.0, 0.7, 1.7, 2.8, 4.9, and 8.5 GPa (Supporting Information, Figure S9). Figure 2c,d shows the variations of lattice constants and unit-cell volume with pressure, and all the lattice constants are listed in the Supporting Information, Table S1. Distinct anisotropic compressibility can be observed (Figure 2c), that the contraction of the c axis is 2.5 times greater than that of the a and b axis before 3 GPa. In comparison with the less compressible inorganic sublattice, the interlayer organic cations exhibit high compressibility along the layer stacking direction (c axis) at low pressures. Above 4 GPa, a near isotropic compression was observed. Thus, the relationship between the unit-cell volume and pressure was fitted in two regions (below 3 GPa and above 4 GPa) using the second-order Birch–Murnaghan equation of state (EOS; see details in the Supporting Information). The obtained B_0 value is much smaller in the low-pressure region than that in the high-pressure region, indicating a typical two-step compression nature of the 2D halide perovskites.^[10a]

When the applied pressure exceeded 10 GPa, significant structural disordering occurred, as evidenced by the appearance of a broad diffuse background and the disappearance of Bragg diffraction peaks. As the pressure was further increased to 28 GPa, all the diffraction peaks disappeared, indicating an amorphous phase. Upon decompression, an irreversible

structural evolution was observed, and the amorphous character could exist as low as 3 GPa, which is probably because the rigid inorganic framework could more easily recover than the soft organic component with decreasing pressure.^[10b] This behavior results in the highly disordered inorganic sublattices, which gives rise to a blueshift of the absorption edge.^[10a,d] The disappearance of several diffraction rings in XRD images (Supporting Information, Figure S10a,b) after pressure treatments suggests that a higher crystallographic symmetry than that of the original sample is obtained.^[8b] As shown in the Supporting Information, Figure S10c, the structure of the decompressed sample can be fitted into a monoclinic $P2/m$ crystal structure with $a = 11.03 \text{ \AA}$, $b = 15.27 \text{ \AA}$, $c = 4.39 \text{ \AA}$, and $\beta = 90.230^\circ$. The Raman results in the Supporting Information, Figure S11 provide further evidence for the different behaviors of $(\text{HA})_2(\text{GA})\text{Pb}_2\text{I}_7$ during compression and decompression, which affects the atomic and electronic configurations after high-pressure treatments. The detailed discussion can be found in the Supporting Information. Such structural irreversibility is responsible for the irreversible variations of the optical properties of $(\text{HA})_2(\text{GA})\text{Pb}_2\text{I}_7$ under high pressures.

DFT calculations were performed to understand the interplay between the crystal structures and electronic structures under high pressure. The calculated electronic band structure in Figure 3a demonstrates the direct band gap nature at the Γ point of $(\text{HA})_2(\text{GA})\text{Pb}_2\text{I}_7$ at ambient conditions. The valence band maximum (VBM) with hybrid characteristics mainly originates from antibonding interactions of I 5p and a small amount of Pb 6s, while the

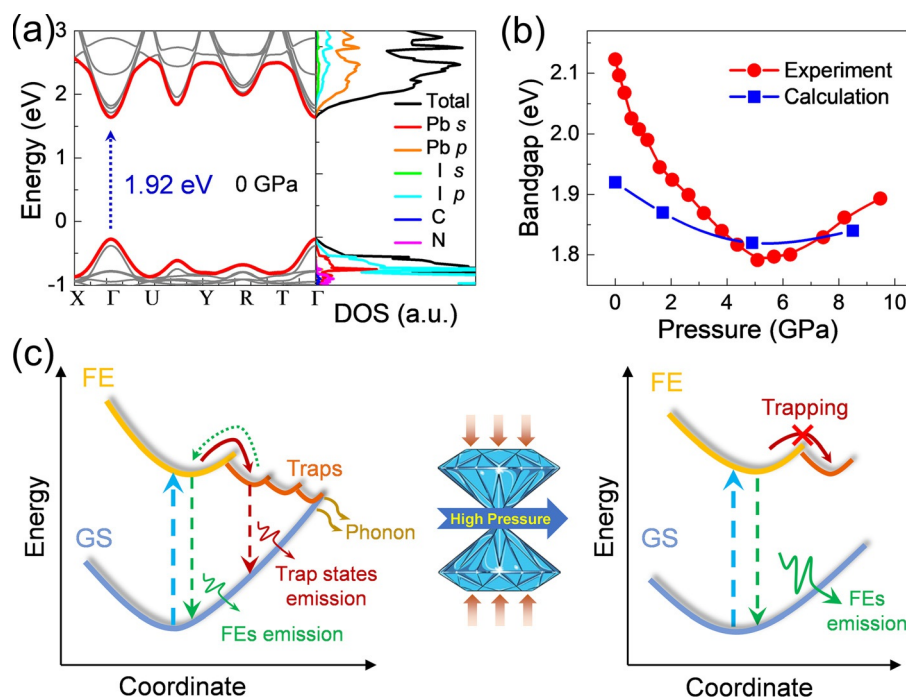


Figure 3. DFT calculations of $(\text{HA})_2(\text{GA})\text{Pb}_2\text{I}_7$ and mechanisms of emission enhancement under high pressures. a) Calculated band structures and the partial density of states (PDOS) from each element at ambient conditions. b) The calculated band gap as a function of pressure in comparison with the experimental results. c) Diagram of the pressure-induced anomalous variations and the underlying mechanisms. Ground state (GS), free-exciton state (FE), and trapped states (Traps).

conduction band minimum (CBM) is dominated by the Pb 6p orbitals. The calculated band structures and partial density of states (PDOS) of $(\text{HA})_2(\text{GA})\text{Pb}_2\text{I}_7$ at representative pressures of 1.7 GPa, 4.9 GPa, and 8.5 GPa are shown in the Supporting Information, Figure S12. The calculated band gap first decreases with pressure up to 5 GPa and then increases with further pressurization (Figure 3b), which is in line with the experimentally observed redshift followed by a blue-shift from the UV/Vis absorption spectroscopy (Figure 1e). The mechanism of the pressure-induced anomalous variations in $(\text{HA})_2(\text{GA})\text{Pb}_2\text{I}_7$ is illustrated in Figure 3c. A close correlation between the nonradiative recombination and the nature of A-site cations in 2D perovskites through exciton-phonon interactions was revealed that reducing these interactions can lead to a higher emission.^[5] Because of the large GA cations, a strong exciton-phonon interaction in the heavily distorted inorganic sublattice results in the excitons to be localized, that is, the formation of overmuch trapped excitons at ambient conditions. These trapped states would induce excessive nonradiative recombination by phonon-assisted energy transfer.^[6,7,14] With increasing pressure, the lattice contraction leads to phonon hardening which considerably reduces the exciton-phonon interaction and, thus, enlarges the potential barrier for carrier trapping.^[3a,7,15] Therefore, the photogenerated carriers can hardly form the trapped states and the

nonradiative recombination pathway is primarily blocked, resulting in an enhanced emission with more symmetric line-shape from the free excitons.

During decompression, the obtained amorphous yellow phase is not luminescent until the pressure is released to around 1.5 GPa, when a light-induced irreversible transformation can occur. The evolution of the PL spectra excited by 405 nm laser is displayed in Figure 4a, where the exposure time of each curve is 1 second in succession. Surprisingly, the PL intensity is dramatically enhanced under the laser irradiation, accompanying a color change from yellow to orange, as shown in the inset of Figure 4a. Thus, interestingly, we can use laser beam to draw a pattern on the surface of the yellow sample in the DAC chamber, like laser engraving. Figure 4b shows the optical and fluorescence images of the laser-irradiated sample at 1.5 GPa with the “HP” pattern drawn on the surface, which clearly demonstrates the transformation from the non-luminescent yellow phase to the luminescent orange phase triggered by laser irradiation. In contrast, the light-induced phase transition did not occur when we changed the laser from 405 nm to 532 nm, since the absorption edge of the sample released to 1.5 GPa is 460 nm (Supporting Information, Figure S4). This suggests that the above-band gap excitation (using 405 nm laser) provides enough driving force for the transition from the yellow phase

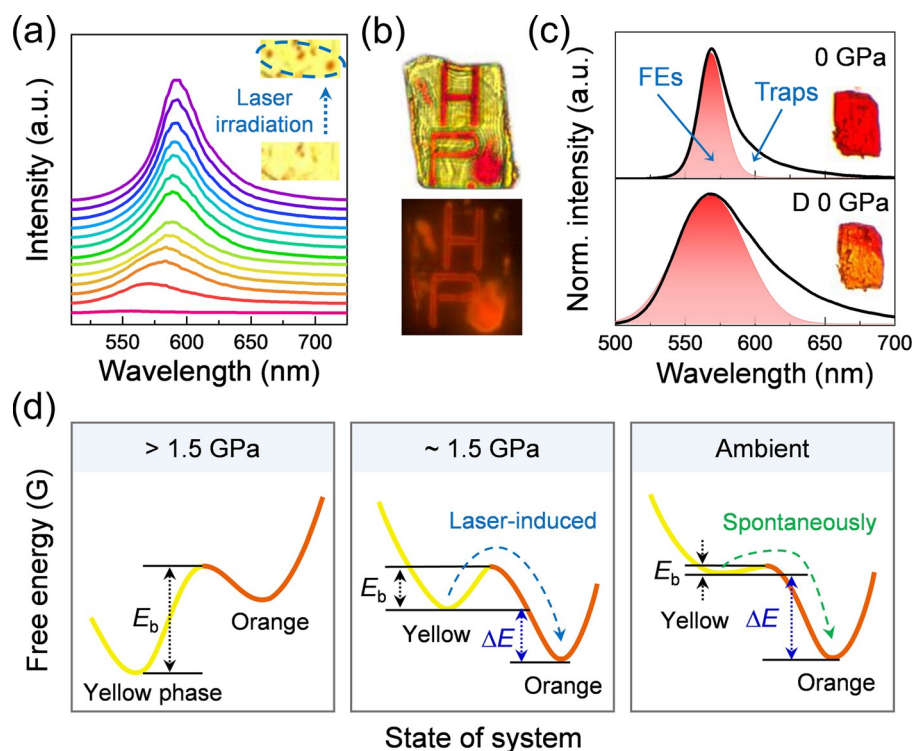


Figure 4. Anomalous variations of the optical properties in $(\text{HA})_2(\text{GA})\text{Pb}_2\text{I}_7$ during decompression. a) Evolution of the PL spectra over time excited by 405 nm laser at around 1.5 GPa during decompression, the exposure time of each curve is 1 second in succession. The inset shows the optical images before and after laser exposure. b) Optical and fluorescence images of the laser-irradiated sample at 1.5 GPa with the “HP” pattern drawn on the surface, which suggests the transformation from a non-luminescent yellow phase to a luminescent orange phase triggered by laser irradiation. c) The fitted PL spectra before and after the high-pressure treatments, where the red and white regions are the contributions from the FEs and the trapped states, respectively. d) Illustration of the energetic variations and photophysical processes during decompression. E_b indicates the energetic barrier for the transition between the amorphous yellow phase and the crystalline orange phase; ΔE denotes the thermodynamic energy difference of these two phases.

to the orange phase, while the below-band gap irradiation (using 532 nm laser) cannot overcome the energetic barrier between these two phases. Also, note that the above-band gap excitation cannot trigger the phase transition at higher pressures (for example, > 3 GPa), as shown in the Supporting Information, Figure S13. These results suggest that pressure can change the height of the energetic barrier between these two phases and even further reverse their energetic order, therefore pressure-induced phase transitions could enable the generation of novel materials.

A well-known example of the pressure-induced change in energetic stability is the preparation of diamond from graphite under high pressure and high temperature. High pressure reverses the energetic order of these two carbon allotropes, making diamond thermodynamically more stable than graphite under high pressure, and the high temperature provides the driving force to overcome the energetic barrier for the conversion. In our case, pressure acts in two ways: it reverses the sign of the free energy difference (ΔG) between the yellow and orange phases; and reduces the energy barrier (E_b) for the phase transformation. As illustrated in Figure 4d, the yellow phase is energetically more stable in the high-pressure region. When the pressure decreases to a certain value (ca. 1.5 GPa in this case), it becomes metastable and could transform to a new phase in orange color by above-band gap laser irradiation (405 nm) which can provide enough driving force to overcome the energetic barrier. The energy barrier becomes much shallower when further decompressed to ambient conditions, and the yellow phase can spontaneously transform into the orange phase with thermal vibrations in the lattice.

In high-pressure research on materials sciences, pressure is utilized to tune and improve properties by adjusting the thermodynamic features away from their ground states, in a bid to reach new states with superior properties that could be preserved at ambient conditions.^[8b,13] Impressively, this new orange phase of $(\text{HA})_2(\text{GA})\text{Pb}_2\text{I}_7$ obtained by the recrystallization of the pressure-induced amorphous phase exhibits a significantly enhanced PL by over 100% compared to the original sample (Supporting Information, Figure S14 and Table S2). The carrier trapping via exciton-phonon interaction might be suppressed in the pressure-regulated structure of the orange phase, resulting in an enhanced PL with a more symmetric peak. We fitted the PL spectra to estimate the contributions of the FEs emission and the trap-states emission of the original sample and pressure-treated sample, as shown in Figure 4c and summarized in the Supporting Information, Table S2. The reduction of trapped states by 17% was observed for the sample after pressure treatments, leading to a two-fold enhancement of the emission. This agrees well with the relationship between the PL intensity and the FEs contribution revealed during compression (Supporting Information, Figure S15). The aforementioned pressure-induced amorphization and recrystallization processes generate a new orange phase with higher crystallographic symmetry (Supporting Information, Figure S10). This would result in the reduction of carrier trapping and, thus, achieve a significantly enhanced emission in comparison to the initial sample. It is of great significance

to retain novel materials discovered at high pressures, just like the high-pressure/temperature synthesis of the diamond from graphite, compression of 0D CdSe nanoparticles into luminescent 1D nanowires,^[13] and pressure sintering of MAPbBr_3 nanocrystals into highly luminescent nanoplates.^[16] Pressure provides an alternative clean and efficient way to manipulate the atomic and electronic structures, and therefore, will further our fundamental understandings and inspire scientists to develop more high-performance optoelectronic materials at ambient conditions.

Conclusion

A significantly enhanced emission was achieved in 2D halide perovskite $(\text{HA})_2(\text{GA})\text{Pb}_2\text{I}_7$ under high pressures, reaching a 12-fold increment at 1.59 GPa in comparison with that at ambient conditions. Using various in situ experimental characterization and first-principles calculations, the enhancement was demonstrated to be related to the pressure-induced suppression of carrier trapping. Furthermore, during decompression, an irreversible and anomalous process was revealed where an amorphous phase of $(\text{HA})_2(\text{GA})\text{Pb}_2\text{I}_7$ with a higher band gap in yellow was obtained that is non-luminescent. Intriguingly, the emission can be triggered and dramatically increased under above-band gap laser irradiation when the pressure was released to a certain value (1.5 GPa), accompanied by a color change from yellow to orange. Impressively, such an orange phase obtained via the recrystallization of the pressure-induced amorphous phase is stable at ambient conditions, which emits a significantly stronger PL by over 100% compared to the original sample. Our results demonstrate that pressure can not only deepen our fundamental understandings of the structure–property relationship in halide perovskites but could also enable the development of novel materials with enhanced properties. Particularly, pressure changes the height of the energetic barrier between different phases and even reverses the energetic order, and therefore enables the generation of new materials through pressure-induced phase transitions.

Acknowledgements

This work is supported by the National Nature Science Foundation of China (NSFC) (Grant Nos. 51527801 and U1530402). The in situ high-pressure XRD measurements were performed at HPCAT (Sector 16), Advanced Photon Source (APS), Argonne National Laboratory (ANL). HPCAT operations are supported by DOE-NNSA's Office of Experimental Sciences. The high-pressure Raman measurements were performed at GeoSoilEnviroCARS (The University of Chicago), APS, ANL. GeoSoilEnviroCARS is supported by the National Science Foundation—Earth Sciences (EAR-1634415), Department of Energy GeoSciences (DE-FG02-94ER14466), and partially by COMPRES through NSF Cooperative Agreement EAR-1661511. The APS is a user facility operated for the DOE Office of Science by ANL under Contract DE-AC02-06CH11357. The syn-

thesis of 2D perovskite single crystals is supported by the U.S. Department of Energy, Office of Basic Energy Sciences, Division of Materials Sciences and Engineering, under award DE-FG02-09ER46664 to S.J., Y.F., and M.P.H. The authors appreciate the language editing by Editor Freyja O'Toole.

Conflict of interest

The authors declare no conflict of interest.

Keywords: carrier trapping · high-pressure chemistry · phase transitions · photoluminescence enhancement · 2D halide perovskites

- [1] a) S. D. Stranks, G. E. Eperon, G. Grancini, C. Menelaou, M. J. Alcocer, T. Leijtens, L. M. Herz, A. Petrozza, H. J. Snaith, *Science* **2013**, *342*, 341–344; b) M. A. Green, A. Ho-Baillie, H. J. Snaith, *Nat. Photonics* **2014**, *8*, 506–514; c) M. Grätzel, *Nat. Mater.* **2014**, *13*, 838–842; d) H. Zhu, Y. Fu, F. Meng, X. Wu, Z. Gong, Q. Ding, M. V. Gustafsson, M. T. Trinh, S. Jin, X. Y. Zhu, *Nat. Mater.* **2015**, *14*, 636–642; e) M. V. Kovalenko, L. Protesescu, M. I. Bodnarchuk, *Science* **2017**, *358*, 745–750; f) T. Leijtens, K. A. Bush, R. Prasanna, M. D. McGehee, *Nat. Energy* **2018**, *3*, 828–838; g) L. N. Quan, B. P. Rand, R. H. Friend, S. G. Mhaisalkar, T. W. Lee, E. H. Sargent, *Chem. Rev.* **2019**, *119*, 7444–7477; h) Y. Cao, N. Wang, H. Tian, J. Guo, Y. Wei, H. Chen, Y. Miao, W. Zou, K. Pan, Y. He, H. Cao, Y. Ke, M. Xu, Y. Wang, M. Yang, K. Du, Z. Fu, D. Kong, D. Dai, Y. Jin, G. Li, H. Li, Q. Peng, J. Wang, W. Huang, *Nature* **2018**, *562*, 249–253; i) J. Luo, X. Wang, S. Li, J. Liu, Y. Guo, G. Niu, L. Yao, Y. Fu, L. Gao, Q. Dong, C. Zhao, M. Leng, F. Ma, W. Liang, L. Wang, S. Jin, J. Han, L. Zhang, J. Etheridge, J. Wang, Y. Yan, E. H. Sargent, J. Tang, *Nature* **2018**, *563*, 541–545.
- [2] a) T. C. Sum, N. Mathews, *Energy Environ. Sci.* **2014**, *7*, 2518–2534; b) B. Saparov, D. B. Mitzi, *Chem. Rev.* **2016**, *116*, 4558–4596.
- [3] a) L. Mao, C. C. Stoumpos, M. G. Kanatzidis, *J. Am. Chem. Soc.* **2019**, *141*, 1171–1190; b) C. Katan, N. Mercier, J. Even, *Chem. Rev.* **2019**, *119*, 3140–3192.
- [4] a) Y. Fu, H. Zhu, J. Chen, M. P. Hautzinger, X. Y. Zhu, S. Jin, *Nat. Rev. Mater.* **2019**, *4*, 169–188; b) M. D. Smith, H. I. Karunadasa, *Acc. Chem. Res.* **2018**, *51*, 619–627.
- [5] X. Gong, O. Voznyy, A. Jain, W. Liu, R. Sabatini, Z. Piontkowski, G. Walters, G. Bappi, S. Nokhrin, O. Bushuyev, M. Yuan, R. Comin, D. McCamant, S. O. Kelley, E. H. Sargent, *Nat. Mater.* **2018**, *17*, 550–556.
- [6] Y. Fu, M. P. Hautzinger, Z. Luo, F. Wang, D. Pan, M. M. Aristov, I. A. Guzei, A. Pan, X. Zhu, S. Jin, *ACS Cent. Sci.* **2019**, *5*, 1377–1386.
- [7] X. Wu, M. T. Trinh, D. Niesner, H. Zhu, Z. Norman, J. S. Owen, O. Yaffe, B. J. Kusch, X. Y. Zhu, *J. Am. Chem. Soc.* **2015**, *137*, 2089–2096.
- [8] a) A. P. Drozdov, P. P. Kong, V. S. Minkov, S. P. Besedin, M. A. Kuzovnikov, S. Mozaffari, L. Balicas, F. F. Balakirev, D. E. Graf, V. B. Prakapenka, E. Greenberg, D. A. Knyazev, M. Tkacz, M. I. Eremets, *Nature* **2019**, *569*, 528–531; b) X. Lü, Y. Wang, C. C. Stoumpos, Q. Hu, X. Guo, H. Chen, L. Yang, J. S. Smith, W. Yang, Y. Zhao, H. Xu, M. G. Kanatzidis, Q. Jia, *Adv. Mater.* **2016**, *28*, 8663–8668; c) C. Ji, B. Li, W. Liu, J. S. Smith, A. Majumdar, W. Luo, R. Ahuja, J. Shu, J. Wang, S. Sinogeikin, Y. Meng, V. B. Prakapenka, E. Greenberg, R. Xu, X. Huang, W. Yang, G. Shen, W. L. Mao, H.-K. Mao, *Nature* **2019**, *573*, 558–562; d) Y. Wang, X. Lu, W. Yang, T. Wen, L. Yang, X. Ren, L. Wang, Z. Lin, Y. Zhao, *J. Am. Chem. Soc.* **2015**, *137*, 11144–11149; e) X. Lü, W. Yang, Q. Jia, H. Xu, *Chem. Sci.* **2017**, *8*, 6764–6776; f) Q. Li, Z. Chen, B. Yang, L. Tan, B. Xu, J. Han, Y. Zhao, J. Tang, Z. Quan, *J. Am. Chem. Soc.* **2020**, *142*, 1786–1791; g) J. Lin, H. Chen, Y. Gao, Y. Cai, J. Jin, A. S. Etman, J. Kang, T. Lei, Z. Lin, M. C. Folgueras, L. N. Quan, Q. Kong, M. Sherburne, M. Asta, J. Sun, M. F. Toney, J. Wu, P. Yang, *Proc. Natl. Acad. Sci. USA* **2019**, *116*, 23404–23409; h) P. Postorino, L. Malavasi, *J. Phys. Chem. Lett.* **2017**, *8*, 2613–2622; i) M. Szafranski, A. Katrusiak, *J. Phys. Chem. Lett.* **2017**, *8*, 2496–2506; j) G. Liu, L. Kong, W. Yang, H.-k. Mao, *Mater. Today* **2019**, *27*, 91–106.
- [9] a) Z. Ma, Z. Liu, S. Lu, L. Wang, X. Feng, D. Yang, K. Wang, G. Xiao, L. Zhang, S. A. T. Redfern, B. Zou, *Nat. Commun.* **2018**, *9*, 4506; b) Y. Shi, Z. Ma, D. Zhao, Y. Chen, Y. Cao, K. Wang, G. Xiao, B. Zou, *J. Am. Chem. Soc.* **2019**, *141*, 6504–6508; c) Y. Fang, L. Zhang, L. Wu, J. Yan, Y. Lin, K. Wang, W. L. Mao, B. Zou, *Angew. Chem. Int. Ed.* **2019**, *58*, 15249–15253; *Angew. Chem.* **2019**, *131*, 15393–15397.
- [10] a) G. Liu, J. Gong, L. Kong, R. D. Schaller, Q. Hu, Z. Liu, S. Yan, W. Yang, C. C. Stoumpos, M. G. Kanatzidis, H. K. Mao, T. Xu, *Proc. Natl. Acad. Sci. USA* **2018**, *115*, 8076–8081; b) S. Liu, S. Sun, C. K. Gan, A. G. Del Aguila, Y. Fang, J. Xing, T. T. H. Do, T. J. White, H. Li, W. Huang, Q. Xiong, *Sci. Adv.* **2019**, *5*, eaav9445; c) T. Yin, B. Liu, J. Yan, Y. Fang, M. Chen, W. K. Chong, S. Jiang, J. L. Kuo, J. Fang, P. Liang, S. Wei, K. P. Loh, T. C. Sum, T. J. White, Z. X. Shen, *J. Am. Chem. Soc.* **2019**, *141*, 1235–1241; d) L. Zhang, L. Wu, K. Wang, B. Zou, *Adv. Sci.* **2019**, *6*, 1801628.
- [11] A. Jaffe, Y. Lin, C. M. Beavers, J. Voss, W. L. Mao, H. I. Karunadasa, *ACS Cent. Sci.* **2016**, *2*, 201–209.
- [12] C. C. Stoumpos, D. H. Cao, D. J. Clark, J. Young, J. M. Rondinelli, J. I. Jang, J. T. Hupp, M. G. Kanatzidis, *Chem. Mater.* **2016**, *28*, 2852–2867.
- [13] B. Li, K. Bian, X. Zhou, P. Lu, S. Liu, I. Brener, M. Sinclair, T. Luk, H. Schunk, L. Alarid, P. G. Clem, Z. Wang, H. Fan, *Sci. Adv.* **2017**, *3*, e1602916.
- [14] Y. Fu, X. Jiang, X. Li, B. Traore, I. Spanopoulos, C. Katan, J. Even, M. G. Kanatzidis, E. Harel, *J. Am. Chem. Soc.* **2020**, *142*, 4008–4021.
- [15] M. P. Hautzinger, D. Pan, A. K. Pigg, Y. Fu, D. J. Morrow, M. Leng, M.-Y. Kuo, N. Spitha, D. P. Lafayette, D. D. Kohler, J. C. Wright, S. Jin, *ACS Energy Lett.* **2020**, *5*, 1430–1437.
- [16] T. Yin, Y. Fang, W. K. Chong, K. T. Ming, S. Jiang, X. Li, J. L. Kuo, J. Fang, T. C. Sum, T. J. White, J. Yan, Z. X. Shen, *Adv. Mater.* **2018**, *30*, 1705017.

Manuscript received: January 31, 2020

Revised manuscript received: May 13, 2020

Accepted manuscript online: July 5, 2020

Version of record online: August 13, 2020